Experimental Study of the Role of the Weber and Capillary Numbers on Mesler Entrainment

John. R. Saylor and Garrett D. Bounds
Dept. of Mechanical Engineering, Clemson University, Clemson, SC 29634

DOI 10.1002/aic.13764
Published online February 23, 2012 in Wiley Online Library (wileyonlinelibrary.com).

Mesler entrainment is the formation of a very large number of very small bubbles by a relatively low velocity drop impacting a liquid surface. The role of the Weber number in Mesler entrainment has received significant attention. However, the effect of the capillary number, which quantifies the relative importance of viscous and surface tension forces, has not been explored. This is due primarily to the fact that virtually all Mesler entrainment research has used a single liquid, water, as the working fluid. This, combined with certain experimental restrictions, makes difficult an independent variation of the Weber and capillary numbers. To address this problem, Mesler entrainment was investigated using two silicone oils, having kinematic viscosities of 0.65 cSt and 10.0 cSt, respectively, revealing the effect of the capillary number on Mesler entrainment, a result which has not been obtained heretofore. The silicone oils give extremely repeatable results when compared to water. © 2012 American Institute of Chemical Engineers *AIChE J,* 58: 3841–3851, 2012
Keywords: bubble phenomena, fluid mechanics, interfacial processes

Introduction

Mesler entrainment is the production of a large number of very small bubbles, caused by the relatively low velocity impact of a drop with a flat liquid interface. An example image of Mesler entrainment due to the authors is presented in Figure 1. This image was taken from beneath the liquid surface to reveal the formation of bubbles. It is generally understood that these bubbles are formed when a very thin film of air is trapped between the approaching drop and the liquid surface. This air film subsequently collapses to form a myriad of small bubbles. Careful observation of Figure 1b reveals bubbles concentrated in lines radiating outward from the bottom most portion of the bubble pattern. This chandelier-like structure is typical of Mesler entrainment, although not universally observed.

Mesler entrainment was first documented by Russell Mesler who was attempting to explain observations of higher heat transfer rates associated with boiling in thin films.[1–3] Mesler discovered that, in thin liquid films, new boiling nucleation sites often occurred where a bubble had recently risen to the surface and popped.[4] Bergman and Mesler[5] showed that this occurred in thick films of liquid as well. Exactly why these new nucleation sites formed was not clear. Carroll and Mesler[6] hypothesized that it is the drops formed when a rising bubble pops that are responsible for the new nucleation sites. Specifically, they postulated that these drops subsequently hit the gas/liquid interface, entrain air bubbles which propagate to the liquid/solid interface, and then form new nucleation sites. These authors used high speed photography to observe low velocity drop impacts and found that they formed many bubbles that were entrained into the liquid bulk by a vortex. They also showed that a bubble sitting on the surface, once popped, caused the formation of drops which then impacted the liquid surface and formed bubbles. A more detailed photographic study by Esmailizadeh and Mesler[7] showed the path taken by the small bubbles formed during a low velocity drop impact, demonstrating how a vortex can transport these bubbles into the bulk. Finally, Sigler and Mesler[8] conducted a photographic study that showed how the air film between the drop and liquid bulk was trapped during the drop impact and suddenly collapsed, resulting in a chandelier style pattern of bubbles like those seen in Figure 1b. Mesler entrainment has also been studied by several other authors, typically in an attempt to understand the overall problem of bubble formation which occurs when a drop impacts a water surface.[9–12] A more detailed review of work on Mesler entrainment can be found in Mills et al.[13]

Thoroddsen et al.[11] conducted a photographic study of bubble formation caused by drop impacts. Several experiments presented in their work were for conditions wherein Mesler entrainment is expected to occur. Thoroddsen's study is unique, in that it was conducted using a one million fps camera, resulting in image sequences that temporally resolve the formation of the air film between the drop and bulk fluid, and the subsequent collapse of that film to form bubbles. Figures 7a and 8a of their work reveal bubble formation that is almost certainly Mesler entrainment based on the bubble formation pattern and the Weber number. In Figure 8a of that work, the authors show how the air film collapse progresses from one side of the impact region to the other, leaving bubbles just behind the collapse locations. Furthermore, although the spatial resolution of their camera did not permit

Correspondence concerning this article should be addressed to J. R. Saylor at jsaylor@clemson.edu.

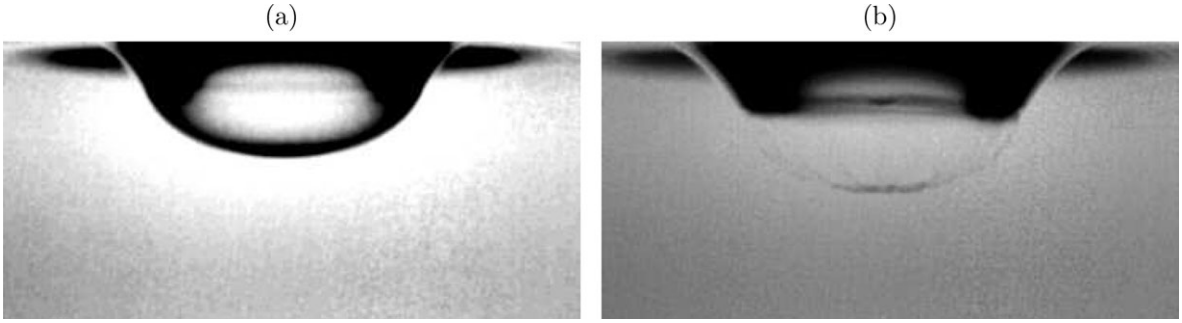

Figure 1. Sample image of Mesler entrainment.

(a) Crater caused by drop impact, just prior to formation of bubbles. (b) Mesler entrainment bubbles as observed 1 ms after image presented in (a). Careful observation reveals that the bubbles are organized in a chandelier style pattern. Note that these images are obtained with the camera pointing slightly upward from beneath the surface. Hence, nothing above the free surface is visible (including the drop) due to total internal reflection. The liquid used in these images was silicone oil having a kinematic viscosity of 10.0 cSt.

visualization of the smallest bubbles, these authors estimate the bubble diameters in this water study were as small as 15 μm, and that $\sim$5000 bubbles are formed during a single drop impact.

Assuming that the parameters that control Mesler entrainment are the liquid density, ρ, the liquid viscosity, μ, the drop diameter d, the impact velocity V, the surface tension σ, and the acceleration due to gravity, g, the Buckingham Pi theorem shows that three-dimensionless groups will describe the Mesler entrainment phenomenon. These three groups are typically written as the Weber, Froude, and capillary numbers, defined as

$$\mathrm{We} = \frac{\rho d V^2}{\sigma} \tag{1}$$

$$\mathrm{Fr} = \frac{V^2}{gd} \tag{2}$$

and

$$\mathrm{Ca} = \frac{\mu V}{\sigma}, \tag{3}$$

respectively. Of course, it is reasonable to assume that the viscosity and density of the surrounding gas may also play a role in this process, adding two additional dimensionless groups. However, investigation of these groups is left for future work.

The capillary number is expected to affect Mesler entrainment since it has been shown to have an effect on other types of bubble entrainment. For example, Deng et al.[14] show that Ca affects bubble entrainment in the regular bubble entrainment region. However, the effect of Ca on Mesler entrainment has not been explored.

Of course values for Ca can be obtained from data presented in existing studies of Mesler entrainment. However, this approach is complicated by the fact that virtually all studies of Mesler entrainment have been conducted with water as the working fluid. The only exceptions to this that we are aware of is one paper by Esmailizadeh and Mesler, where the liquids 1-butanol, n-amyl alcohol, glycerol, kerosene, ethylene glycol, methanol, and isopropyl alcohol were investigated.[7] This was a photographic study, however, photographs were not presented of the bubble entrainment for any of these liquids, and the authors only revealed that in these fluids, the bubbles formed were smaller, and that there were less of them. The fact that Mesler entrainment has been studied using essentially only one working fluid means that, in these studies, the fluid properties are fixed in the definitions of We and Ca, and hence, We/Ca $\sim Vd$. Furthermore, in experimental work of this type, it is difficult to generate a large range in drop diameter. Very small drops are difficult to detach from a needle, and drops do not remain attached to the needle long enough to make large drops, or these large drops break up while falling. Hence, effectively, We/Ca $\sim V$ for the water experiments that have been conducted to date. This means that in the We vs Ca parameter space, data from existing studies falls on a single curve.

To ameliorate the situation described above, two new working fluids were chosen for study in this experimental work. Specifically, two silicone oils were chosen. The properties of these silicone oils are presented along with those of water in Table 1. The first silicone oil was chosen to have properties such that We and Ca would be similar to that explored in previous water studies, specifically the work of Mills et al.[13] This was done to ascertain whether anomalous results on water might be due to difficulties in maintaining surface cleanliness (see below). The second silicone oil was chosen to have a kinematic viscosity much larger than that of the first silicone oil (about 15 times larger). These two silicone oils will be referred to hereinafter via their kinematic viscosity; the first silicone oil having a kinematic viscosity of $v = 0.65$ cSt, and the second having $v = 10.0$ cSt. As in most experiments of this kind, the impact velocity V was varied by releasing drops of nominally constant diameter from a range of heights. The resulting parameter space, as well as that due to Mills et al.[13] (using water), is presented in Figure 2, showing that, at constant We, significantly different values for Ca are explored by using these two silicone oils.

It would be desirable, if possible, to use the data obtained herein to also explore the effect of the Froude number on

Table 1. Kinematic Viscosity, Density and Surface Tension of The Two Silicone Oils Explored, as Well as Water

Liquid	v (cSt)	ρ (kg/m^3)	σ (N/m)
#1	0.65	757.9	0.0159
#2	10.00	932.5	0.0201
H_2O	0.91	997.0	0.0721

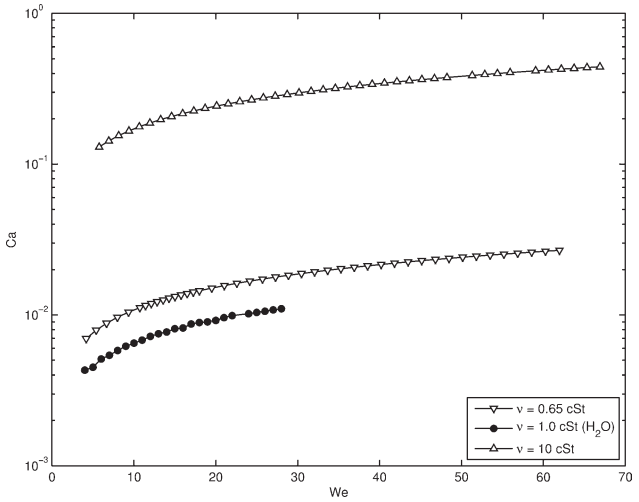

Figure 2. Parameter space explored in this research on capillary vs Weber number coordinates.

The solid symbols are data obtained from the water experiments of Mills et al.[13] Each symbol represents a data point that will be plotted in the next section.

Mesler entrainment. However, there are no fluid properties in the definition of Fr. Thus, varying Fr independently of We and Ca would require independent variation of d and V, which is challenging for the reasons presented above. The parameter space explored here is presented in Figure 3 on Fr vs We coordinates, revealing an essentially linear relationship between Fr and We for the conditions of the present work, which prevents an independent assessment of the role of Fr.

Water is a very unique and challenging liquid to use in experimental studies of interfacial phenomena like bubble formation. This is mainly because water surfaces are extremely difficult to maintain in a clean state due to the very large number of naturally occurring substances which will form monolayers on water surfaces. When studying problems like bubble formation in water, it is very difficult to know if the observed behavior is that of pure water, or that of water contaminated by an unknown or poorly quantified surfactant monolayer. Many authors have noted a lack of reproducibility when studying Mesler entrainment in water. In an attempt to avoid contamination problems associated with water, Mills et al.[13] purposely contaminated the water with the soluble surfactant Triton X-100. This was done to both the drop water and the bulk water. The goal was to create a system where sufficient surfactant was present on the water surface that contaminating surfactants would play a negligible role. However, even under these conditions, for the values of We where Mesler entrainment was observed, it was never observed with 100% repeatability. Indeed, when observed, the repeatability was at best less than 80%. Accordingly, a secondary motivation of the present work was to ascertain if the repeatability of Mesler entrainment improves when using liquids not susceptible to contamination from adventitious surfactants. As silicone oils are very resistant to surfactant contamination, it is hypothesized that repeatability will be improved in these liquids.

In addition to its relevance to boiling, Mesler entrainment is important to the study of transport across the air/water interface of lakes, rivers, and oceans. In these situations, the large number of small bubbles that occur during Mesler entrainment would serve to enhance gas exchange, heat transfer, and evaporation. Mesler entrainment could occur from the small diameter, low impact velocity splash drops created by raindrop impacts, by bubbles popping at the surface, and from wave breaking events. Transport due to small Mesler bubbles would be particularly effective because their low buoyancy force would enable these bubbles to remain in the water for long periods of time without rising to the surface. Understanding the conditions during which Mesler entrainment occurs is necessary to include this phenomenon in models of gas exchange and heat transfer in rivers, lakes, and oceans.

Experimental Method

The experimental setup used to conduct these experiments is illustrated in Figure 4. The apparatus used to release drops was constructed of plastic tubing press-fit into a 30 gauge hypodermic needle. The needle was prepared by grinding flat the beveled tip to ensure consistent snap off dynamics for all drops. The drop fluid was contained in a Hamilton 25 mL GasTight syringe and the flow of the drop fluid was controlled by a Cole-Parmer 74900 series syringe pump. An interval of 1–2 min was maintained between drops to allow the free surface to return to a steady condition and to allow sufficient time for any bubbles which may have formed to rise to the surface and burst. Both the dropping apparatus and reservoir were placed on vertical traverses to provide accurate control of the drop release height and vertical position of the free surface without altering the camera optics.

Two Dow Corning 200 Series silicone liquids were used in these experiments. Liquid #1 (CAS # 107-46-0, Sigma-Aldrich) had a kinematic viscosity $v = 0.65$ cSt and was selected to approximately match the kinematic viscosity of water. The kinematic viscosity of liquid #2 (CAS # 63148-62-9, Sigma-Aldrich) was $v = 10$ cSt and was chosen to obtain a capillary number Ca outside the range of what has presently been explored in Mesler entrainment research. The kinematic viscosity, density, and surface tension are presented in Table 1 for these two liquids as well as for water.

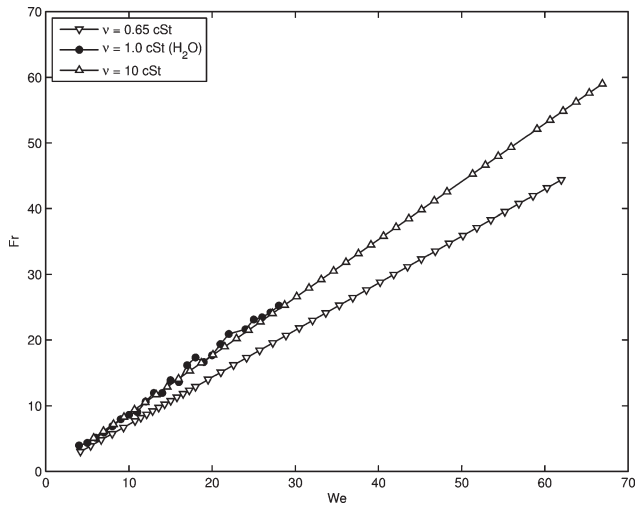

Figure 3. Parameter space explored in this research on Froude vs Weber number coordinates.

The solid symbols are data obtained from the water experiments of Mills et al.[13]

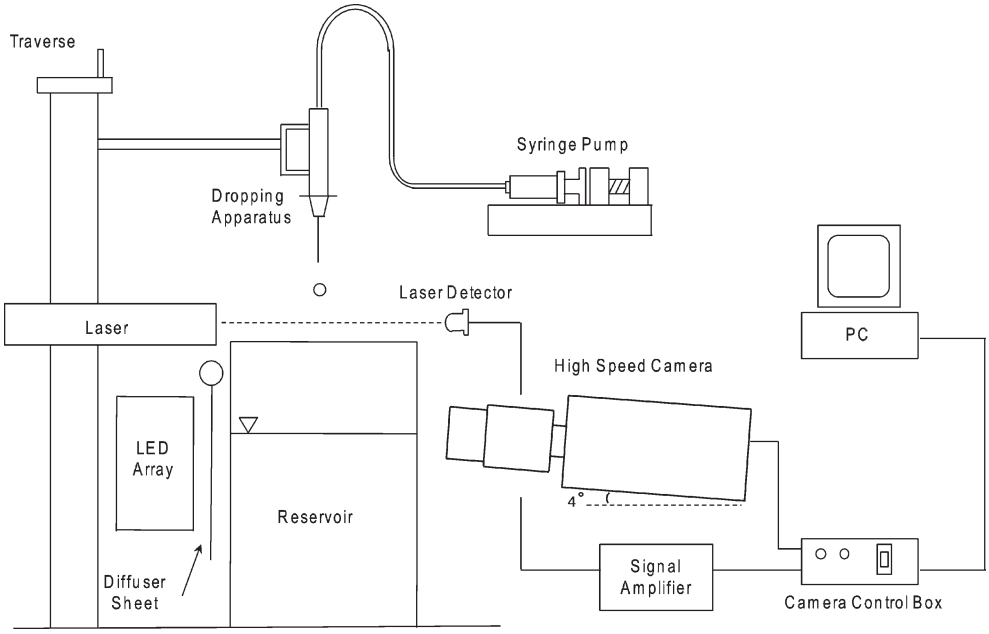

Figure 4. Experimental apparatus.

In all experiments, the same liquid was used for the drop and reservoir.

The drop release height was measured relative to a datum established by touching the needle to the free surface of the silicone oil in the reservoir. The drop height was measured relative to this position on the vertical traverse, to which the needle was attached. The drop release heights ranged from 6.0 to 43.0 mm for the 0.65 cSt liquid and from 8.0 mm to 50.0 mm for the 10 cSt liquid. Drop release heights were typically increased in 1 mm increments. The silicone oil reservoir was constructed of Plexiglas having a thickness of 9 mm. The tank height, width, and depth were 17.7, 8.2, and 8.2 cm, respectively. The volume of the working fluid placed in the tank was ~770 mL.

Images were captured using a Cooke pco.1200hs high speed camera. The camera was positioned below the free surface and pointed upward at an angle of 4°. Because of total internal reflection, only subsurface events could be seen in this orientation, and hence the drop itself was not visible. The camera was paired with a Canon 65 mm macro lens. The camera permitted image storage of arbitrary subregions of the CCD array. A 400 × 480 pixel region was used for the main data set. For this set of images, the framing rate was 1060 fps, the magnification was 1×, the exposure time was 120 μs, and the pixel resolution was 11 μm. An additional data set was taken for each of the working fluids to explore a specific range in We (see below). For this additional data set, a 400 × 360 pixel region was recorded at 1400 fps, 2× magnification and an 80 μs exposure time. The pixel resolution for these images was 5.5 μm.

Image acquisition was initiated manually using the camera software, whereupon an image buffer was continuously overwritten. Image acquisition was terminated a selected number of frames after receipt of an external trigger signal generated when the falling drop passed through a laser beam located horizontally above the bulk liquid surface, as illustrated in Figure 4. To generate this signal, a 4 mW HeNe laser was directed at an LED which was used as an optical detector. The laser beam was oriented horizontally, directly beneath the drop syringe and approximately 10 mm above the water surface. An op-amp was used to amplify the output of the light-emitting diode (LED), and the falling edge of this signal, generated when the falling drop interrupted the laser beam, was used to trigger the camera.

Lighting was provided in a back-lit configuration, using a 8 × 16 array of white LEDs. A sheet of translucent plastic was placed between the LED array and the reservoir to diffuse the light from the LED array, providing more uniform illumination. For drops imaged at 2× magnification, a 20 mW HeNe laser was added to the experimental setup in a side-lit configuration to provide the additional light needed when imaging this smaller field of view and shorter exposure time. For these images, the laser beam was precisely positioned to illuminate the region where bubbles were entrained.

The process used to image the drops began by turning on the LED array and the syringe pump. The camera was then set to begin recording data. After the drop impact, the LED array and syringe pump were turned off. Turning off the syringe pump kept unnecessary drops from disturbing the free surface. Turning off the LED array was a precautionary measure to prevent heating of the bulk fluid by the light source, ensuring that the drop and bulk fluid were at the same temperature.* As will be described in greater detail below, the image sequence acquired for each drop impact event was subsequently reviewed and categorized as: (1) floating drop event, (2) Mesler entrainment event, or (3) neither.

Computing We and Ca requires the drop diameter d and impact velocity V. These quantities were measured during a separate set of experiments, where the optical setup was altered so that the optical axis of the camera was oriented parallel to the water surface enabling acquisition of drop images just prior to impact, thereby allowing measurement of the impact velocity. All other aspects of the experimental setup were unchanged. Images were obtained for both work-

*This was a conservative measure, as the LED array was very efficient and produced only a small amount of heat.

ing fluids over a range of drop heights, allowing measurement of the impact velocity for each drop height. To determine the impact velocity, the centroid of the drop images was computed from the binary version of the initially grayscale image (see below). The y value of the centroid of the three images obtained before impact for the 10 cSt fluid and the four images obtained before impact for the 0.65 cSt fluid were recorded, and a linear fit of these y values vs the time of image acquisition was obtained. One less image was used for the 10 cSt fluid because of the slightly larger drop diameter for this case. For each drop height, images from three runs were used to obtain an average velocity at that height. Data from 19 release heights ranging from 6 to 42 mm were used to obtain an empirical equation for velocity vs release height having the form

$$V = \alpha h^{1/2} + \beta \tag{4}$$

where V is the drop impact velocity (mm/s), h is the drop release height (mm) and α and β are constants. Equation 4 was used to obtain V when calculating We and Ca.

The following image processing steps were applied to convert each grayscale drop image to a binary image. First, each image was cropped to reduce the number of pixels to be analyzed and to reduce potential complications due to variations in the background. Next, the Canny edge detection algorithm[15] was applied to the images, using threshold values obtained via trial-and-error, resulting in an image consisting of a binary outline of the drop. Next, the drop was filled to give a binary, filled image of the drop. Finally, a median filter was applied which was used to detect and eliminate spurious pixels. A sample drop image is presented in Figure 5 showing the initial grayscale image and the final processed binary image. All image processing was done using Mathworks Matlab 2009b. Processed images were saved and the location of the edge was verified by visually comparing the grayscale image and binary image of each drop. Visualization of the images was done using ImageJ.[16]

To compute drop diameter, drops were assumed to be axisymmetric about the vertical axis. Using this assumption, each row of pixels in the binary drop image was considered to be a cylindrical volume having a height of one pixel and a diameter equal to the width of that row of pixels. Summing these volumes yielded the total drop volume, and the drop diameter was computed as that of an equivolume sphere. Averaged over 57 drops for each fluid, the diameters were $d = 1.58$ mm and $d = 1.73$ mm for the 10 and 0.65 cSt fluids, respectively.

Results

As noted above, the image sequences from each drop impact were viewed and categorized as: (1) floating drop event, (2) Mesler entrainment event, or (3) neither. Drops which created on the order of 10–15 bubbles or more upon the breakdown of the drop crater were categorized as Mesler entrainment. Drops that bounced on the free surface (often several times) before coalescing with the bulk were characterized as floating. When <10 bubbles were observed, and no bouncing was observed, the event was categorized as neither. A sample sequence of images is presented in Figure 6 showing the evolution of the crater beneath the drop impact for each of the three event categories.

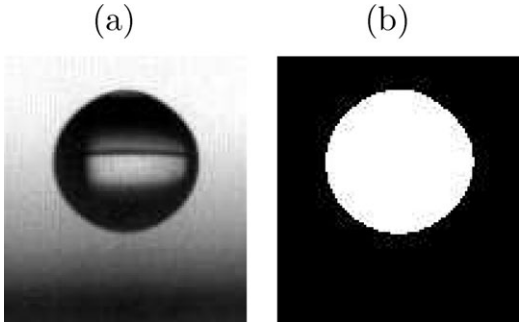

Figure 5. Gray scale image from camera (a) and image after processing (b).

A total of 343 drops were recorded for the 0.65 cSt fluid and 248 drops for the 10 cSt fluid. Following the approach taken by Mills et al.,[13] a frequency f was defined as the fraction of drops at a given We for which Mesler entrainment occurred. That is, f is the number of Mesler entrainment events divided by the total number of drops, at each We. This frequency is plotted in Figure 7 for both fluids explored. Drops were binned in terms of drop release heights, which were separated by 1 mm. This resulted in a Weber number bin size that was slightly different for each of the two silicone oils, but was approximately 1.6 for both.

The results presented in Figure 7 show that, for these silicone oils, Mesler entrainment exhibits "digital" behavior. That is, roughly speaking, the drop events either show Mesler entrainment 100% of the time or none of the time. For both liquids, as We is increased, there is a rapid transition from $f = 0$ to $f = 1$ for small We. In this region, the behavior changes from having Mesler entrainment 0% of the time to having Mesler entrainment 100% of the time, with a very brief transition zone in between. A similar rapid transition from $f = 1$ to $f = 0$ is observed for large We, going from 100% Mesler entrainment to no Mesler entrainment. The range of Weber numbers where $f = 1$ is $12.8 \leq \mathrm{We} \leq 21.0$ for the 0.65 cSt fluid and $18.7 \leq \mathrm{We} \leq 36.1$ for the 10.0 cSt fluid.

The lower, $f = 0 \rightarrow 1$ transition occurs over $11.4 < \mathrm{We} < 12.8$ for the 0.65 cSt fluid and over $16.0 < \mathrm{We} < 18.7$ for the 10.0 cSt fluid. The upper, $f = 1 \rightarrow 0$ transition occurs over $21.0 < \mathrm{We} < 22.6$ for the 0.65 cSt liquid and over $36.1 < \mathrm{We} < 42.1$ for the 10.0 cSt liquid.

As noted above, the results presented in Figure 7 show very "digital" behavior for Mesler entrainment in these silicone oils. This behavior is very different from that observed in water, where all researchers have observed that Mesler entrainment occurs sporadically under the best of conditions. This is best revealed in Figure 8, where the data presented in Figure 7 is replotted with the data obtained from the water experiments of Mills et al.[13] As this plot shows clearly, a value of $f = 1$ is never attained for the water data, achieving a maximum of less than 0.8. The results of Mills et al.[13] were attained using water mixed with the soluble surfactant Triton X-100, in an attempt to provide a surface that is purposely contaminated with a surfactant, and thereby, less subject to contamination by environmental surfactants. Nevertheless, repeatable Mesler entrainment was still never attained. A possible explanation for the difference between water and the silicone oils studied here is presented in the Discussion section.

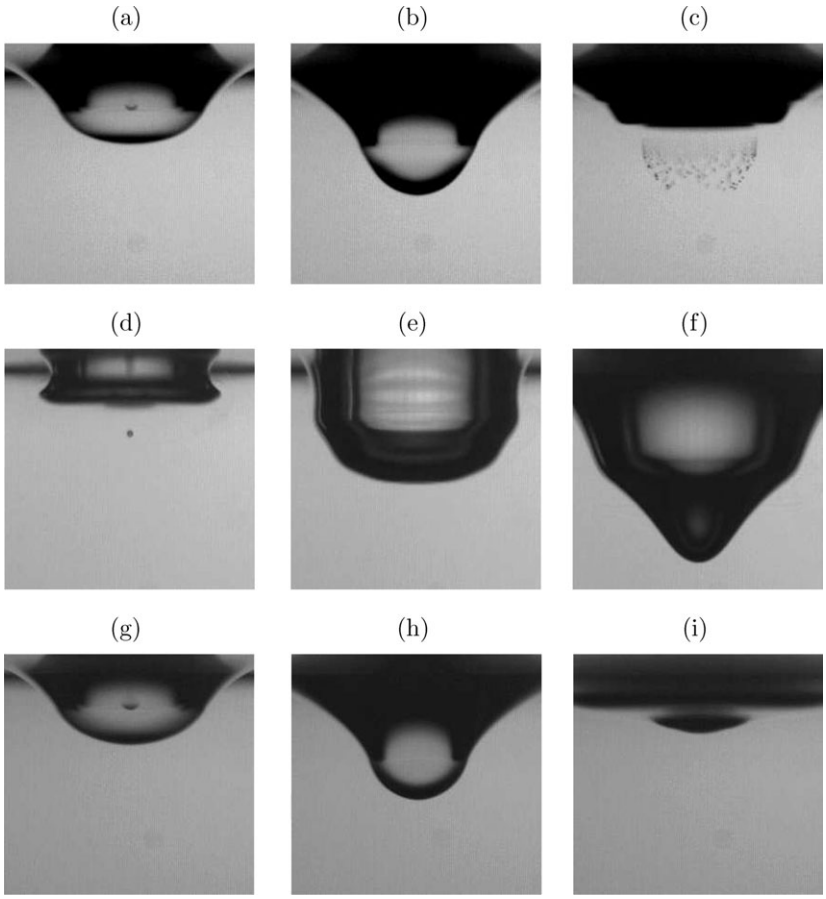

Figure 6. Images representative of each of the three impact classifications: a–c Mesler entrainment, d–f neither, g–i floating drops.

Each image is 3.1 mm wide and 3.0 mm high.

Figure 8 suggests an effect of viscosity on Mesler entrainment. The initial rise in f begins at We = 11.4 for the 0.65 cSt fluid and at We = 21.0 for the 10.0 cSt fluid, a difference of 9.6 in We. Moreover water, which has a kinematic viscosity of 1.0 cSt displays its initial rise in f at a Weber number close to that of the 0.65 cSt silicone oil. In an attempt to collapse the data of all three liquids, f was plotted against $\mathrm{We/Ca}^{1/n}$, where n was adjusted iteratively in integer increments to attain maximal collapse. This was achieved at $n = 9$, and the results are presented in Figure 9, showing reasonably good collapse of the low Weber number transition region for all of the fluids. We note that the above

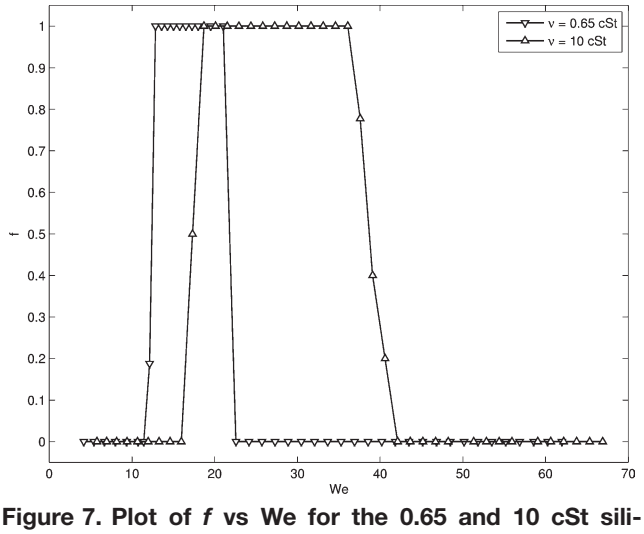

Figure 7. Plot of f vs We for the 0.65 and 10 cSt silicone liquids.

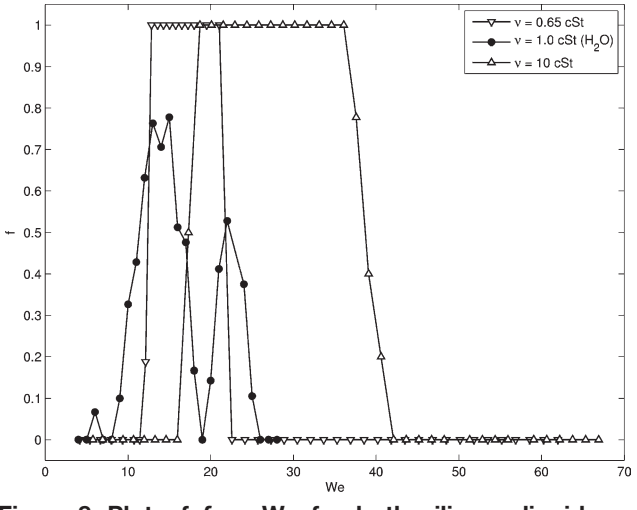

Figure 8. Plot of f vs We for both silicone liquids as well as for the data obtained from the water experiments of Mills et al.[13]

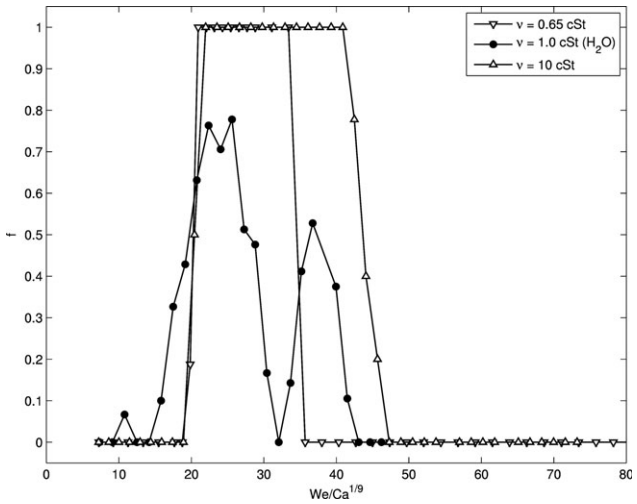

Figure 9. Plot of f vs $\mathrm{We}/\mathrm{Ca}^{\frac{1}{9}}$ for both silicone liquids as well as for the data obtained in the water experiments of Mills et al.[13]

approach is empirical; choice of an exponent guided by theory would be preferable. However, given that the exact instability mechanism by which Mesler entrainment occurs is still unclear, this was not possible. The data for the trailing edge does not collapse and a possible reason for this difference is discussed below.

For these experiments, it was observed that as We increased, the size of the entrained bubbles decreased. At We $\sim$21 for the 0.65 cSt fluid and We $\sim$40 for the 10 cSt fluid, the bubbles became so small that it became difficult to determine whether the drop images contained entrained bubbles. Up until these values of We, classifications of drops could be made simply because the presence or absence of bubbles was readily observed. To minimize the subjectivity of the classification of Mesler entrainment at large We, the following criteria were established and applied to all observed drops in this range. First, a drop had to produce entrained bubbles in the characteristic parabolic-shape formed after the breakdown of the air film which surrounds the drop crater in entrainment events. This parabolic shape can be seen in Figure 12, with a distinctive parabolic shape for each of the two fluids. Second, bubbles which formed near the free surface must have been visible over a series of frames. Observing bubbles over an elapsed period of time verified that they were, in fact, bubbles being observed as they moved in the bulk fluid and not, for example, optical imperfections on the camera lens. This criterion was applied specifically to bubbles formed near the free surface because they were easier to observe than bubbles formed near the center of the parabolic shape. Bubbles of the latter type were more mobile and were often swept into vortex rings, making their whereabouts difficult to discern over a series of frames.

In spite of the above approach, at high We, the bubble size decreased to the pixel resolution of the camera (11 μm). Further increases in We did not seem to result in Mesler entrainment, however, it was impossible to say whether this was because Mesler entrainment had ceased or the bubbles were simply too small to observe. To help resolve this uncertainty, a second set of experiments was conducted where the magnification of the optical system was increased from 1$\times$ to 2$\times$. To generate clear images, the frame exposure time was reduced, and more intense lighting was used in the region of entrainment, as described in the Experimental Method section. The results from these 2$\times$ magnification experiments are presented, along with the original 1$\times$ data, for the 0.65 cSt fluid in Figure 10, and for the 10.0 cSt fluid in Figure 11. From these figures, it can be seen that the same digital pattern is exhibited in the 2$\times$ magnification results, however, the range in We over which entrainment was observed has been extended on the large Weber number side of the plot. The low Weber number side of the plot does not change. This observation is consistent with a bubble diameter that decreases with We since a larger magnification factor enables visualization of smaller bubbles. Evidence of micron scale bubbles was also obtained by Thoroddsen et al.[11] (see Fig. 7b of their paper) at We = 23 when using water as a working fluid. In their work, resolution of the smallest sized bubbles was also not possible. It would be desirable, of course, to further increase the image resolution and determine the lower bound of bubble size, and thereby determine the true upper bound of We for Mesler entrainment. This would be very difficult, however, since at 2$\times$, the pixel resolution is already at 5.5 μm, making further decreases using visible light extremely challenging, especially for the necessarily large working distance of the optical system. It should be noted that the uncertainty in the large Weber number upper bound in these f vs We plots is the reason that it was the lower Weber number bound that was used to optimize the value of n when scaling f to $\mathrm{We}/\mathrm{Ca}^{1/n}$ in Figure 9. It is possible that, if the upper Weber number limit was confidently ascertained, the lower and upper transition regions would collapse when plotting the data as in Figure 9, however this is a supposition at the present time.

Differences existed in the entrainment behavior observed for the 0.65 and 10 cSt fluids. The 0.65 cSt fluid, having a lower viscosity, permitted the formation of drop-induced vortex rings that transported bubbles into the bulk. Vortex rings were not observed in the higher viscosity 10.0 cSt fluid. Bubbles that were formed in this fluid stayed essentially fixed at the location where they were formed upon collapse of the air film. This can be seen in Figure 12 where in images a–d, the formation of the bubbles can be seen, followed by their subsequent propagation by a vortex ring into

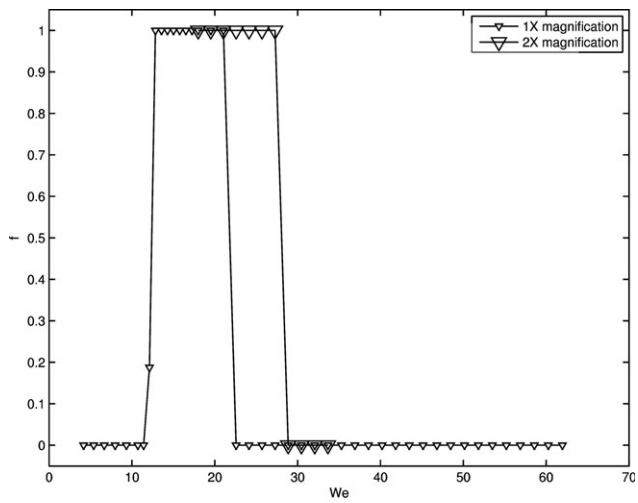

Figure 10. Plot of f vs We for both the original 1$\times$ magnification data and the 2$\times$ data for the ν = 0.65 cSt fluid.

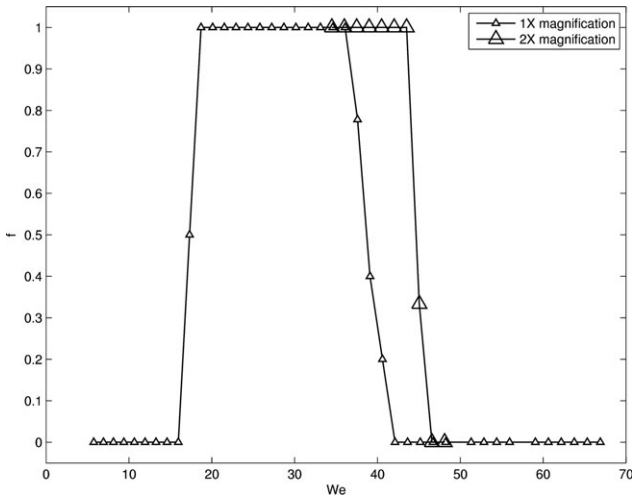

Figure 11. Plot of *f* vs We for both the original 1× magnification data and the 2× data for the ν = 10.0 cSt fluid.

the liquid bulk of the 0.65 cSt fluid. The sequence of events for the 10.0 cSt fluid is presented in frames e–h, where it is apparent that the collapse of the air film which occurs shortly after frame e results in a layer of air bubbles having the same shape as the air film that resided between the drop and bulk fluid only a moment earlier. The parabolic shape of this layer of bubbles remains essentially unchanged, moving only slightly upward.

As noted earlier, the Mesler entrainment results obtained here for silicone oils showed repeatable behavior in the sense that Mesler entrainment occurred either all of the time or none of the time (with the exception of the narrow transitional Weber number regions described above). The Mesler entrainment behavior was also repeatable in the sense that the topology of the crater formation and subsequent bubble formation patterns were very consistent. The sequence of events leading to Mesler entrainment in the 10.0 cSt fluid, seen in Figures 12e–h, occurred virtually identically for all of the data obtained. For the 0.65 cSt fluid, one of two possible sequences occurred. These two sequences are shown in Figure 13. The first of these two sequences, shown in the top row of this figure, shows the formation of a crater (first frame), and the collapse of the air film (second frame) resulting in 10–20 bubbles of varying size. The second sequence of events is shown in the second row where the crater forms (first three frames) and then breaks down into a large number of bubbles of similar diameter. In subsequent frames (not shown here), these bubbles are swept downward in a vortex ring. The sequence seen in the first row was far more common than the second row, but only these two types of behavior were observed. It is unclear why two behaviors were observed in the 0.65 cSt fluid, and why this was the case for the 0.65 cSt fluid and not the 10.0 cSt fluid.

Discussion

An important result of this research is that Mesler entrainment can occur in a highly repeatable fashion, as revealed in Figure 7. Such repeatable results have not been observed for Mesler entrainment heretofore. It is also true that virtually all prior Mesler entrainment work has been conducted using water as the working fluid. Accordingly, a question that this work raises is whether water is a unique fluid in that it does not result in repeatable Mesler entrainment, or whether silicone oil is a unique fluid in that it does result in repeatable Mesler entrainment. To address this question with any degree of certainty would require further experimentation

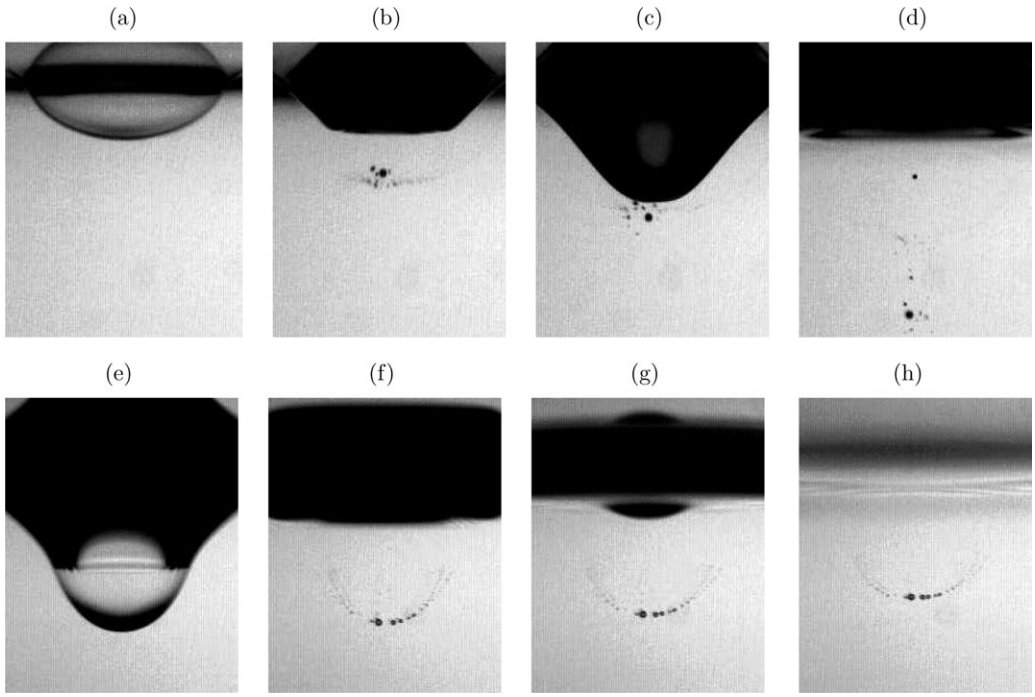

Figure 12. Comparison of the bubble formation pattern for the 0.65 cSt fluid a–d and the 10 cSt fluid e–h.

Each image width and height is 2.3 mm and 3.0 mm, respectively. The time from drop impact for each image is: (a) 1.89 ms, (b) 3.77 ms, (c) 5.66 ms, (d) 12.26 ms, (e) 7.55 ms, (f) 9.44 ms, (g) 11.33 ms, and (h) 17.93 ms.

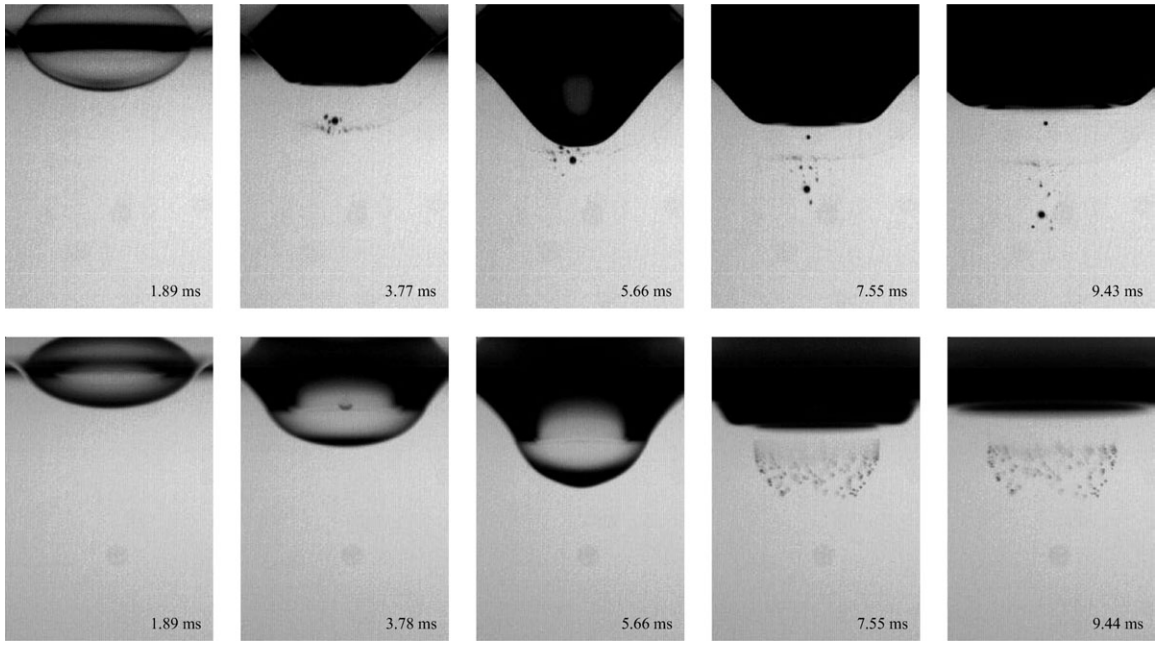

Figure 13. Differences in entrainment behavior observed in the 0.65 cSt fluid.

The top row shows the entrainment type which occurred most often, characterized by 10–15 irregularly sized bubbles. The bottom row shows the more uncommon entrainment type which is similar to entrainment observed in water. Bubbles in this entrainment type are regular in size and more numerous than in the other type with 100–120 bubbles created per drop. Each image width and height is 2.3 mm and 3.4 mm, respectively.

with other liquids. We postulate, however, that water is the unique fluid because water is highly susceptible to surfactant contamination. Without purposeful contamination by surfactants, a water surface becomes contaminated over time by environmental surfactants resulting in a constantly changing surface condition and, hence, irreproducibility. In the work of Mills et al.,[13] the water was purposely contaminated with the soluble surfactant Triton X-100 in an attempt to create a constant ''contaminated'' surface condition. However, even then, variations in surface contamination probably existed. For example, when the drop strikes the water surface, the local surface concentration may change. Moreover, it is not clear whether the same surface concentration exists as a water drop is formed at the nozzle. Perhaps small differences in the time taken to form the drop may result in differences in the concentration of surfactant on the drop surface. Finally, as a water drop falls, oscillations of the drop may result in changes in the surfactant concentration which may vary and affect the probability of Mesler entrainment. Because silicone oils are so much less susceptible to surfactant contamination, such problems do not exist, and it may be that this is the reason for the reproducibility observed for these liquids, but not for water.

An important goal of these experiments was to determine the effect of viscosity on Mesler entrainment. As shown in Figure 9, the f vs We data collapsed reasonably well when the Weber number was scaled as $\boldsymbol{We/Ca^{\frac{1}{3}}}$. This scaling collapses the location of the $f = 0 \rightarrow 1$ transition for both silicone oils and for water as well, although not for the $f = 1 \rightarrow 0$ transition, probably due to resolution issues as discussed in the prior section. Taken as a whole, these results indicate that the viscosity of the liquid is an important parameter, but that Ca is of secondary importance when compared to We.

Liquid drops naturally oscillate as they fall, causing the drop shape to change from prolate to oblate, achieving a spherical shape in between. As a result, drops released from different heights have different shapes upon impact. The effect of drop shape on drop impact phenomena has been studied in other areas. For example, many experiments have shown that drop shape affects vortex formation during drop impact events.[17–22] Mills et al.[13] showed that the shape of the drop at impact affects Mesler entrainment in their water experiments. Specifically, they showed that f increased when the drop was closer to spherical, as opposed to prolate or oblate in shape. Using the equation for the oscillation frequency of a drop at its fundamental harmonic

$$f_d = \frac{4}{\pi}\sqrt{\frac{\sigma}{\rho d^3}} \tag{5}$$

and ignoring air drag to obtain the drop fall velocity, Mills et al.[13] developed the following equation for the number of drop oscillations occurring prior to impact

$$n_{\mathrm{osc}} = \frac{4\sigma}{\pi\rho g d^2}\sqrt{\mathrm{We}} \tag{6}$$

The water data presented in Figure 8 shows that f varies with We in a periodic fashion, exhibiting two peaks; one at We = 15 and another at We = 22. Using the properties for water (with Triton X-100) presented in Mills et al.,[13] one obtains values of n_{osc} at these two peaks that differ by 0.93, almost one full oscillation, supporting the conclusion of those authors that the shape of the drop at impact affects Mesler entrainment. This notwithstanding, the data obtained herein for silicone oils does not show a periodic variation in f with We, at least for the range of We explored herein. As

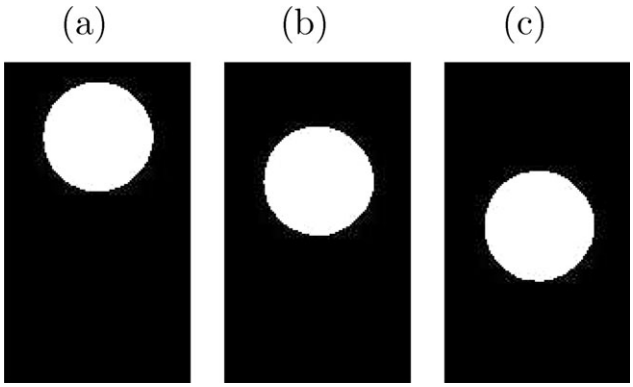

Figure 14. Final three images of a 10 cSt liquid drop prior to impacting the liquid surface.

Each image is 2.7 mm wide by 4.6 mm high, and the time separation between each image is 0.944 ms.

noted above, $f = 1$ for $12.8 \leq \mathrm{We} \leq 21.0$ for the 0.65 cSt fluid and $18.7 \leq \mathrm{We} \leq 36.1$ for the 10.0 cSt fluid. Applying Eq. 6, shows that over these ranges n_{osc} differs by 0.92 oscillations for the 0.65 cSt fluid (almost exactly the same as for the data obtained in the water experiments of Mills et al.[13]), and 1.89 oscillations for the 10.0 cSt fluid. In other words, for both of the silicone oil experiments conducted here, the range in heights from which drops were released was large enough to ensure that the drops impacted the liquid surface for the entire range of possible drop shapes–from oblate to spherical to prolate. Why, then, does not the silicone oil data exhibit a periodic variation in f as does water? A relatively straightforward answer exists for the 10 cSt fluid. This fluid is so viscous that drop oscillations are highly damped. This can be seen in Figure 14 which shows the final three images prior to impact of a 10 cSt drop. Each of these images shows a drop that is very spherical. Drop shape is typically quantified by

$$\alpha = \frac{d_v}{d_h} \tag{7}$$

where d_{v} is the maximum vertical extent of the drop and d_{h} is the maximum horizontal extent of the drop, so a spherical drop would yield $\alpha = 1$. The images presented in Figures 14a–c have values of $\alpha = 0.989$, 0.991, and 0.980, respectively, deviating from spherical by 2% or less in all three images. Hence, for the 10 cSt fluid, the drop is essentially always spherical at impact and therefore there can be no effect of drop shape on Mesler entrainment for this fluid.

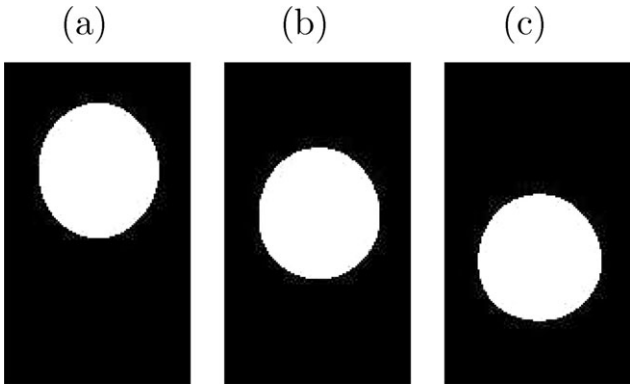

Figure 15. Final three images of a 0.65 cSt drop prior to impacting the liquid surface.

Each image is 2.7 mm wide by 4.6 mm high, and the time separation between each image is 0.944 ms.

For the 0.65 cSt liquid, the drop does change in shape as it falls, as can be observed in Figure 15. For images a–c, $\alpha =$ 1.130, 1.094, and 1.027, a significant variation, and, as noted above, these drops undergo a change in drop shape at impact of 0.92 oscillations over the range of drop release heights explored. Hence, if silicone oil is expected to behave as the water results of Mills et al.[13] suggest, one would expect to see a periodic variation in f in Figure 7, instead of a constant $f = 1$ from $12.8 \leq \mathrm{We} \leq 21.0$. Exactly why this is the case is unclear. It is possible that the shape of the drop at impact still has an effect on bubble entrainment, but it is negligibly small for liquids that do not accrue surfactants (or perhaps only affects the number of bubbles formed or their diameters). For example, it may be that the oscillation of a water drop as it falls modulates the surfactant concentration on the bottom side of the drop to create ideal conditions for entrainment at the phase of the oscillation where the drop is spherical. Further experiments are needed to address this question.

An interesting and unexplained result of this work concerns the $f = 1 \rightarrow 0$ transition which occurs at high Weber numbers. Referring to Figure 7, it is clear that this transition occurs relatively gradually for the 10.0 cSt fluid, when compared to the $f = 0 \rightarrow 1$ transition that occurs for small We. It is tempting to attribute this to spatial resolution issues; that is, as We increases, bubbles get smaller, resulting in values of f between 0 and 1 as the bubbles gradually get too small to see. However, if this was the explanation, then a similar gradual transition would also be observed for the 0.65 cSt fluid. However, this is not the case, and so this observation remains unexplained at this point.

Conclusion

The role of liquid viscosity on the occurrence of Mesler entrainment was quantified via the capillary number. It was demonstrated that the region of onset of Mesler entrainment in plots of percent occurrence were well scaled by the parameter $We/Ca^{\frac{1}{5}}$, a result that has not been obtained prior to this work. This scaling worked reasonably well for two silicone oils and for water. It was also shown that Mesler entrainment is highly repeatable in silicone oils in contrast to water which shows poor repeatability. It is hypothesized that these two different behaviors can be explained by the susceptibility of water to surfactant contamination.

Acknowledgments

The authors thank Robert Teague and John Hicks of the Clemson University Department of Electrical and Computer Engineering for their assistance in conducting these experiments.

Literature Cited

1. Kirby DB, Westwater JW. Bubble and vapor behavior on a heated horizontal plate during pool boiling near burnout. *AIChE Symp Ser*. 1965;61:238–248.
2. Toda S, Ushida H. Study of liquid film cooling with evaporation and boiling. *Heat Transfer Jpn Res*. 1973;2:44–62.
3. Mesler RA. A Mechanism supported by extensive experimental evidence to explain high heat fluxes observed during nucleate boiling. *AIChE J*. 1976;22:246–252.
4. Mesler R, Mailen G. Nucleate boiling in thin liquid films. *AIChE J*. 1977;23:954–957.
5. Bergman T, Mesler R. Bubble nucleation studies. Part I: Formation of bubble nuclei in superheated water by bursting bubbles. *AIChE J*. 1981;27:851–853.

6. Carroll K, Mesler R. Part II: Bubble entrainment by drop-formed vortex rings. *AIChE J*. 1981;27:853–855.
7. Esmailizadeh L, Mesler R. Bubble entrainment with drops. *J Colloid Interface Sci*. 1986;110:561–574.
8. Sigler J, Mesler R. The behavior of the gas film formed upon drop impact with a liquid surface. *J Colloid Interface Sci*. 1990;134:459–474.
9. Oğuz HN, Prosperetti A. Bubble entrainment by the impact of drops on liquid surfaces. *J Fluid Mech*. 1990;219:143–179.
10. Pumphrey HC, Elmore PA. The entrainment of bubbles by drop impacts. *J Fluid Mech*. 1990;220:539–567.
11. Thoroddsen ST, Etoh TG, Takehara K. Air entrapment under an impacting drop. *J Fluid Mech*. 2003;478:125–134.
12. Thoroddsen ST, Etoh TG, Takehara K, Ootsuka N, Hatsuki Y. The air bubble entrapped under a drop impacting on a solid surface. *J Fluid Mech*. 2005;545:203–212.
13. Mills BH, Saylor JR, Testik FY. An experimental study of Mesler entrainment on a surfactant-covered interface: the effect of drop shape and Weber number. *AIChE J*. 2011;58:46–58.
14. Deng Q, Anilkumar AV, Wang TG. The role of viscosity and surface tension in bubble entrapment during drop impact onto a deep liquid pool. *J Fluid Mech*. 2007;578:119–138.
15. Canny J. A computational approach to edge detection. *IEEE Trans Pattern Anal Mach Intell*. 1986;8:679–698.
16. Rasband WS. *ImageJ*, Bethesda, Maryland, USA: National Institutes of Health, 1997–2009.
17. Thomson JJ, Newall HF. On the formation of vortex rings by drops falling into liquids and some allied phenomena. *Proc R Soc Lond*. 1885;39:417–436.
18. Chapman DS, Critchlow PR. Formation of vortex rings from falling drops. *J Fluid Mech*. 1967;29:177–185.
19. Rodriguez F, Mesler R. The penetration of drop-formed vortex rings into pools of liquid. *J Colloid Interface Sci*. 1988;121:121–129.
20. Durst F. Penetration length and diameter development of vortex rings generated by impacting water drops. *Exp Fluids*. 1996;21:110–117.
21. Saylor JR, Grizzard NK. The effect of surfactant monolayers on vortex rings formed from an impacting water drop. *Phys Fluids*. 2003;15:2852–2863.
22. Saylor JR, Grizzard NK. The optimal drop shape for vortices generated by drop impacts: the effect of surfactants on the drop surface. *Exp Fluids*. 2004;36:783–790.

Manuscript received May 18, 2011, and revision received Jan. 23, 2012.